Supporting Information

Chen et al. 10.1073/pnas.1206557109

Materials and Methods

Mice. All experiments were performed under protocols approved by the Animal Care and Use Committee at Massachusetts Institute of Technology and conformed to National Institutes of Health guidelines. For in vivo experiments, two-photon calcium imaging, cell-attached recordings, and single-unit recordings were performed on adult (>6 wk old) C57BL/6 and conditional inositol 1,4,5 trisphosphate receptor type KO (IP_3R2-cKO) mice maintained on a C57BL/6 background. For slice experiments, C57BL/6 mice and IP_3R2-cKO mice aged 2–3 wk (Figs. 3 and 4) and >6 wk (Fig. 5 *A*–*C*) were used. Adult mice were used in the latter experiments to match the ages of IP_3R2-cKO mice used for in vivo experiments. IP_3R2-cKO mice were generated (laboratory of Ken McCarthy, University of North Carolina, Chapel Hill, NC) by (*i*) backcrossing IP_3R2 flox/flox mice (Black Swiss background; Ju Chen, University of California, San Francisco, CA) (1) to C57BL/6J mice (Jackson Laboratory) for four generations to generate mice heterozygous for the floxed IP_3R2 allele (IP_3R2 flox/$^+$) (Fig. S6). The IP_3R2 flox/$^+$ mice were screened by PCR for the retinal degeneration gene known to occur in the IP_3R2 flox/flox background strain (2), which was validated to be absent in these mice. (*ii*) These mice were crossed to GFAP-Cre recombinase mice on a C57BL/6J background to generate IP_3R2 flox/$^+$ mice with or without Cre-recombinase (Fig. S6). (*iii*) These mice were then interbred to generate mice (*iv*) homozygous for the floxed IP_3R2 allele (IP_3R2 flox/flox) and heterozygous for Cre-recombinase (IP_3R2-cKO) (Fig. S6). Mice were genotyped by Transnetyx with real-time PCR using genomic DNA and primers specific to Cre-recombinase (CRE), the 5′ LoxP site of the IP_3R2 floxed allele (*ITPR2* FL), and the WT sequence within the *ITPR2* gene that is disrupted by the insertion of loxP (*ITPR2* WT). The IP_3R2-cKO mice used in our experiments are positive for CRE and *ITPR2* FL but negative for *ITPR2* WT. IP_3R2-cKO mice on the C57BL/6J background were confirmed to have intact visual behavior on a range of visual tests.

In Vivo Surgery. For the in vivo experiments, mice were anesthetized with urethane (1.5 mg/g). In a subset of in vivo calcium imaging experiments, a mixture containing fentanyl (0.05 mg/kg), midazolam (5 mg/kg), and medetomidine (0.5 mg/kg), maintained with 0.2–0.5% isoflurane or fentanyl/medetomidine supplements, was used. Similar conclusions were derived from data collected from experiments using either of the anesthetics. Ophthalmic ointment was used to protect the animal's eyes during surgery and was replaced with silicon oil during imaging. Body temperature was maintained at 37.5 °C with a heating pad. The mice were placed in a stereotaxic apparatus (Kopf Instruments), and bipolar stimulating electrodes were stereotaxically implanted (1.5 mm lateral and 0.5 mm posterior from the bregma, 4.5 mm deep from the surface) in the left nucleus basalis (NB). Two silver wire leads were implanted on the brain's surface, over the left frontal cortex and right visual cortex, respectively, for EEG recordings (performed with an A-M Systems Model 3000 amplifier and a Tektronix TDS 1002 oscilloscope). Desynchronization of the interhemispheric EEG waveform following NB stimulation was used to verify the accuracy of NB electrode implantation in every experiment. A metal headplate was attached to the skull with cyanoacrylate glue and dental acrylic. A 2-mm × 2-mm craniotomy was made over the primary visual cortex (V1), which was later covered with a thin layer of 2% (wt/vol) agarose in artificial cerebrospinal fluid [ACSF; 140 mM NaCl, 5 mM KCl, 2 mM $CaCl_2$, 1 mM $MgCl_2$, 0.01 mM EDTA, 10 mM Hepes, 10 mM glucose (pH 7.4)].

In Vivo Two-Photon Calcium Imaging. A glass pipette filled with 1.0 mM Oregon Green 488 Bapta-1-AM (OGB1-AM) and 100 μM sulforhodamine101 (SR101; Molecular Probes) was visually guided into layer 2/3 using a micromanipulator (MP-285; Sutter Instruments), and a small volume was pressure-injected using a picospritzer. Atropine (500 μM; Sigma) was pressure-injected with a pipette containing Alexa Fluor 594 (A594; Molecular Probes) for visualization of pipette and drug delivery. In vivo imaging of OGB1-AM and SR101 was performed with a two-photon laser scanning microscope (Sutter Instruments) at an excitation wavelength of 810 nm. Fluorescence was detected using photomultiplier tubes (R6357; Hamamatsu). A 25×, 0.95-N.A. lens (Olympus Optical) was used. Image acquisition was carried out in image planes separated by at least 20 μm using ScanImage software (Karel Svoboda Lab, HHMI Janelia Farm). Imaged cells were located at a depth of 120–200 μm below the pial surface.

In Vivo Calcium Imaging data Analysis. Custom-written software in MATLAB (MathWorks) was used for computation of the time-lapse change in fluorescence normalized by the baseline fluorescence (ΔF/F) for each distinct region of interest (ROI). Astrocytes were discriminated from neurons by SR101 labeling, and their ROIs were manually selected on the OGB1-AM fluorescence image. The raw fluorescence intensity was smoothed with a Gaussian kernel, and the ΔF/F was computed for each ROI. The baseline fluorescence was defined as the average fluorescence across prestimulus frames, whereas the change in fluorescence was computed as the baseline fluorescence subtracted from the maximum fluorescence intensity during the stimulus (visual or NB electrical stimulation). Pre-NB and post-NB responses were computed as described in Fig. S2.

In Vivo Cell-Attached Recording. Glass pipettes (1.5-mm tip size, 3–7 MΩ) filled with A594 and held at positive pressure were visually guided into V1 with a two-photon microscope and directed to 100–200 μm below the pial surface (layer 2/3) using a micromanipulator (3). The resistance of the pipette was monitored during the penetration by delivering −0.5-nA current pulses for 6.3 ms at 0.55 Hz with Clampex software (version 8.1; Axon Instruments) and an Axoclamp-2A amplifier (Axon Instruments). When a seal with a cell was obtained during the advancement of pipette (assessed by the increase in pipette tip resistance) and well-isolated spikes were detected on Clampex software during visual stimuli presentation, sustained negative pressure was applied (0.2–0.6 psi) to secure the seal (4). Recordings were performed at a sampling rate of 30 KHz and filtered between 300 Hz and 10 KHz. The pClamp data were analyzed with Clampfit software (version 10.2; MDS Analytical Technologies) for spike detection, and the analyzed data were then imported in MATLAB and further analyzed with custom-written scripts to calculate firing rates in epochs with and without visual stimulus presentation.

Single-Unit Recording. Single-unit extracellular recordings were made using tungsten microelectrodes (1.5–2 MΩ; FHC) as described by Dragoi et al. (5). Briefly, the signal was amplified using an eight-channel differential amplifier (FHC), thresholded using an online amplitude discriminator, displayed on an oscilloscope (TDS 2022B; Tektronix), and played over an audio monitor (Optimus). Units were isolated from the superficial layers of V1 and amplified (Plexon Neurotechnology Research Systems). Offline analysis to sort waveforms for each unit was performed using commercial programs (Offline Sorter version 2.8.8; Plexon, Inc.);

postprocessing was done using in-house code written in MATLAB. In Fig. 6 *C* and *D* and Fig. S8, average normalized responses were calculated by first normalizing the responses to the conditioned (or any unconditioned) orientation by the mean of the responses across all orientations, excluding conditioned (or any unconditioned) orientation before and after NB stimulation. The normalized pre-NB baseline response was then subtracted from the normalized responses in each post-NB time segment. Only visually responsive units (evaluated using a paired *t* test over 8–10 cycles) were used in the analysis. Data points in Fig. 6*D* and Fig. S8 *C* and *D* were computed as sliding window averages of normalized responses.

NB Stimulation. The NB was stimulated with either a single brief train of 50 pulses (0.1 ms per pulse) at 100 Hz (Fig. 2 *A–F*) or multiple trains of these pulses (Figs. 1 *D–F*, 5*D*, and 6) using a stimulator with a constant current stimulus isolation unit (S88 Stimulator; Grass Technologies) or personal computer-driven current isolator (A365; WPI). Visual and NB stimulation were paired by synchronizing the initiation of visual stimulus and output of current isolator through a MATLAB-driven setup.

Visual Stimulation. Visual stimuli, generated with the Psychophysics toolbox (6) in MATLAB, were displayed on a 19-inch liquid crystal display monitor situated 15 cm from the eyes. Random orientation gratings were presented in the calcium imaging and cell-attached recording experiments (Figs. 1 *D–F*, 2 *D–F*, and 5*D*), whereas specific orientation gratings were presented in the single-unit recording experiments (Fig. 6). The onset of the visual stimulus was synchronized to the initiation of acquisition of two-photon calcium images, cell-attached, and single-unit spike recordings. The random orientation grating stimuli consisted of square wave drifting gratings at 100% contrast in eight randomly permuted directions, each 45° apart and lasting for 450 ms. In the calcium imaging experiments, this stimulus was presented for 8 s before alternating with a blank gray screen for 8 s across multiple cycles. The duration was shortened to 4 s in cell-attached recording experiments. In the single-unit stimulus-specific plasticity experiments, multiple trials of a set of nine orientations, each at 4-s intervals at 20° apart, were shown before and after paired NB and specific orientation grating stimulation. A blank gray screen was shown for 4 s between each orientation grating. During the pairing, a specific orientation grating, synchronized to the NB stimulation, was presented every 2 s.

Acetylcholinesterase Histochemistry. At the end of in vivo experiments, mice were supplemented with the fentanyl/medetomidine or urethane anesthesia and perfused transcardially with saline followed by chilled 4% (wt/vol) paraformaldehyde in 0.1 M PBS. The brains were then postfixed in 4% (wt/vol) paraformaldehyde in 0.1 M PBS (<4 °C) overnight. The fixed brains were sectioned into 100-μm horizontal slices with a vibratome and stained for acetylcholinesterase. Slices were incubated in 4 mM acetylthiocholine iodide, 4 mM copper sulfate, and 16 mM glycine in a 50-mM sodium acetate solution (pH 5.0) overnight and developed in 1% (wt/vol) sodium sulfide solution (pH 7.0) for 10 min. Images were captured with an Axiovert 200 microscope (Zeiss) with a Sony 3 CCD color video camera.

Slice Physiology. Coronal visual cortical sections (300 μm) slices were cut in <4 °C ACSF, with 95% O_2/5% CO_2 (pH 7.33–7.38), with a vibratome (VT 1200S; Leica) and incubated in ACSF (room temperature) for at least 30 min before being transferred to a slice chamber for patch recordings. ACSF contained 127 mM NaCl, 25 mM $NaHCO_3$, 2.5 mM KCl, 1.25 mM NaH_2PO_4, 25 mM glucose, 1 mM $MgCl_2$, and 2 mM $CaCl_2$. For postnatal 16 (p16) and older animals, the slicing buffer was prepared by altering the ACSF $CaCl_2$ and $MgCl_2$ concentrations to 1 mM and 5 mM, respectively, to optimize the slice viability. For slice calcium imaging, the slices were preincubated in ACSF containing 1 mM OGB1-AM, 0.4% pluronic F-127 in DMSO, and 95% O_2/5% CO_2 for 45 min before they were rinsed in fresh ACSF for 30 min and transferred to the slice chamber. In a subset of the calcium imaging experiments, the slices were incubated for 10 min in slicing buffer containing 1 μM SR101, which preferentially loads astrocytes (7), before being transferred to fresh ACSF for 10 min. A solution containing OGB1-AM (344 μM), 1.8% (wt/vol) pluronic F-127, and 3.87% (wt/vol) DMSO in ACSF was pressure-puffed to load the calcium indicator in a localized area of astrocytes and neurons. The slices were then incubated in fresh ACSF for 45 min before imaging. All experiments were performed in ACSF except for astrocyte-mediated NMDA current experiments (Fig. 4), where Mg^{2+}-free ACSF with TTX (1 μM) was used. The intracellular pipette solution for patching neurons contained 100 mM potassium gluconate, 20 mM KCl, 10 mM Hepes, 4 mM MgATP, 0.3 mM NaGTP, 10 mM naphosphocreatine, and 295 mM mOSm (pH 7.4), whereas that used for patching astrocytes contained 50 mM K-gluconate, 2 mM ATP, 0.4 mM GTP, 10 mM Hepes, and 310–315 mM mOsm (pH 7.2–7.25). A594 (40 μM) and/or 1,2-Bis(2-aminophenoxy)ethane-*N*,*N*,*N*′,*N*′-tetraacetic acid (BAPTA; 50 mM) was included in this solution in experiments in which the spread of A594 and/or BAPTA in the syncytium was quantified. ACh, atropine sulfate (atropine), scopolamine hydrobromide (scopolamine), TTX, and ATP were purchased from Sigma; D-2-Amino-5-phosphonovaleric acid, 2,3-dihydroxy-6-nitro-7-sulfamoyl-benzo[f]quinoxaline-2,3-dione, and BAPTA were purchased from Tocris. Drugs were bath-applied, except for ACh, which was applied by pressure injection in specific experiments, and BAPTA and A594, which were patch-loaded. In a subset of astrocyte BAPTA/A594 experiments, ATP (20 mM) or ACh (10 mM) was applied by pressure injection at the start of the experiment to check for the health of the slice and viable cellular responses. BAPTA dialysis into astrocytes was only performed in slices that showed astrocyte calcium responses to these agonists. Control experiments for the BAPTA astrocyte dialysis experiments were performed, where BAPTA was puffed into the extracellular space while both spontaneous and ACh-induced slow currents were recorded (Fig. S5*D*).

Analysis of Slow Currents. To avoid possible controversies regarding the definition of slow inward currents, we used the following criteria in Fig. 4, Fig. S5, and Table S1: Both the spontaneous and ACh-induced slow currents were discriminated from standard miniature excitatory postsynaptic currents, such that the former had a time course at least twofold greater than the latter. These slow currents were similar to the slow inward currents observed in the hippocampus (8).

Calcium Imaging in Slices. Layer 2/3 cells were visualized with a Zeiss Axioskop under a Zeiss Achroplan 40× water immersion lens, infrared-differential interference contrast (DIC) optics, and a Streampix 4.20 (Norpix)-driven Retiga Exi CCD camera (Qimaging). Fluorescence was continuously excited using a metal halide lamp (X-CITE 120Q, Lumen Dynamics Group Inc.). OGB1-AM and SR101 were imaged with a blue excitation filter/green emission filter and a green excitation filter/red emission filter, respectively. Images were continuously acquired at a magnification of 2.5× or 4×, 10–20 Hz, using 2 × 2 or 4 × 4 binning. Images were saved by the Streampix software as tagged image file format files and analyzed with custom-written MATLAB scripts. Individual cells were circled manually, in which astrocytes were discriminated from neurons by their morphology, small soma size, and SR101 labeling. The mean fluorescence for each cell was computed from frame to frame, giving a time-varying intensity signal for each cell. After correction for lamp flicker noise and dye photobleaching, ΔF/F was calculated by subtracting the local corresponding baseline (F) from the peak of the response to get

ΔF before taking the ratio by F. Increases in ΔF/F in ROIs indicated an increase in Ca^{2+} concentration.

Immunohistochemistry. For anti-GFAP and neuronal nuclei (NeuN) immunohistochemistry after slice calcium imaging experiments (Fig. 2*H*), the acute slices were fixed with 4% (wt/vol) formaldehyde (in PBS) overnight. The fixed slices were then blocked in 10% (vol/vol) normal goat serum with 1% (vol/vol) Triton in PBS (1 h at room temperature) and stained for rabbit anti-GFAP (1:200, G9269; Sigma) and mouse anti-NeuN (1:250, MAB377; Millipore) overnight (<4 °C). This was followed by a 3-h incubation in Alexa Fluor 488 goat anti-rabbit (1:200, A11034; Invitrogen) and Alexa Fluor 405 goat anti-mouse (1:200, A31553; Invitrogen) before being mounted on a glass slide with Vectashield Hardset mounting media (Vector Labs). The slides were imaged using a confocal microscope (LSM 5 Pascal Exciter; Zeiss). For antimuscarinic AChR, anti-GFAP, and DAPI immunohistochemistry (Fig. S3 *A* and *B*), 50-μm fixed slices were prepared (as described in *SI Materials and Methods*, *Acetylcholinesterase Histochemistry*). The primary antibodies used were rabbit anti-M1, anti-M2 (1:200, AB5164 and AB5166; Millipore), and mouse anti-GFAP (1:400; Sigma), whereas the secondary antibodies were Alexa Fluor 488 goat anti-rabbit (1:200, A11034; Invitrogen) and Alexa Fluor 647 goat anti-mouse (1:200, A21236, Invitrogen). The mounting media contained DAPI (H-1500; Vector Labs). For anti-IP_3R2 and anti-GFAP immunohistochemistry (Fig. 5*A*), 40-μm fixed slices were prepared. The primary antibodies used were rabbit anti-IP_3R2, (1:20, AB3000; Millipore) and mouse anti-GFAP (1:400, G3893; Sigma), whereas the secondary antibodies were Alexa Fluor 488 goat anti-rabbit (1:250, A11034; Invitrogen) and Alexa Fluor 633 goat anti-mouse (1:250, A21236; Invitrogen).

Intracellular Recording in Slices. Glass pipettes (3–5 MΩ) were pulled with a Sutter P80 puller (Sutter Instruments). Layer 2/3 cells were visualized with a Zeiss Axioplan microscope coupled with an Achroplan 40× water immersion lens, infrared-DIC optics, and a Streampix 4.20 (Norpix)-driven infrared Coolsnap cf2 CCD camera (Photometrics). Regular spiking excitatory neurons were identified according to the following morphological and electrophysiological characteristics: pyramidal-shaped soma, apical dendrites radially projecting toward the pial and basal dendrites directed downward and laterally (9), and adaptation of spike frequency when stimulated with a constant current (10). For BAPTA experiments, passive astrocytes were identified by their small round soma with thin radiating processes revealed by A594 filling, highly negative membrane potential, and passive responses to a series of depolarizing steps. Recordings were performed with an Axopatch 200 amplifier (Molecular Devices) with pClamp software in both the current- and voltage-clamp modes. Analysis was performed with Clampfit 10.2.0.12 software.

Statistical Analyses. Statistical analyses of experiments to assess significance were conducted with two-tailed Student *t* tests. Unpaired *t* tests are indicated as *t* tests in the main text. Wilcoxon rank-sum tests were used in Fig. 6 because the populations were not normally distributed.

1. Li X, Zima AV, Sheikh F, Blatter LA, Chen J (2005) Endothelin-1-induced arrhythmogenic Ca2+ signaling is abolished in atrial myocytes of inositol-1,4,5-trisphosphate (IP3)-receptor type 2-deficient mice. *Circ Res* 96:1274–1281.
2. Clapcote SJ, Lazar NL, Bechard AR, Wood GA, Roder JC (2005) NIH Swiss and Black Swiss mice have retinal degeneration and performance deficits in cognitive tests. *Comp Med* 55:310–316.
3. Runyan CA, et al. (2010) Response features of parvalbumin-expressing interneurons suggest precise roles for subtypes of inhibition in visual cortex. *Neuron* 67:847–857.
4. Joshi S, Hawken MJ (2006) Loose-patch-juxtacellular recording in vivo—A method for functional characterization and labeling of neurons in macaque V1. *J Neurosci Methods* 156:37–49.
5. Dragoi V, Sharma J, Sur M (2000) Adaptation-induced plasticity of orientation tuning in adult visual cortex. *Neuron* 28:287–298.
6. Brainard DH (1997) The Psychophysics Toolbox. *Spat Vis* 10:433–436.
7. Nimmerjahn A, Kirchhoff F, Kerr JND, Helmchen F (2004) Sulforhodamine 101 as a specific marker of astroglia in the neocortex in vivo. *Nat Methods* 1:31–37.
8. Perea G, Araque A (2005) Properties of synaptically evoked astrocyte calcium signal reveal synaptic information processing by astrocytes. *J Neurosci* 25:2192–2203.
9. DeFelipe J, Fariñas I (1992) The pyramidal neuron of the cerebral cortex: Morphological and chemical characteristics of the synaptic inputs. *Prog Neurobiol* 39:563–607.
10. Connors BW, Gutnick MJ (1990) Intrinsic firing patterns of diverse neocortical neurons. *Trends Neurosci* 13:99–104.

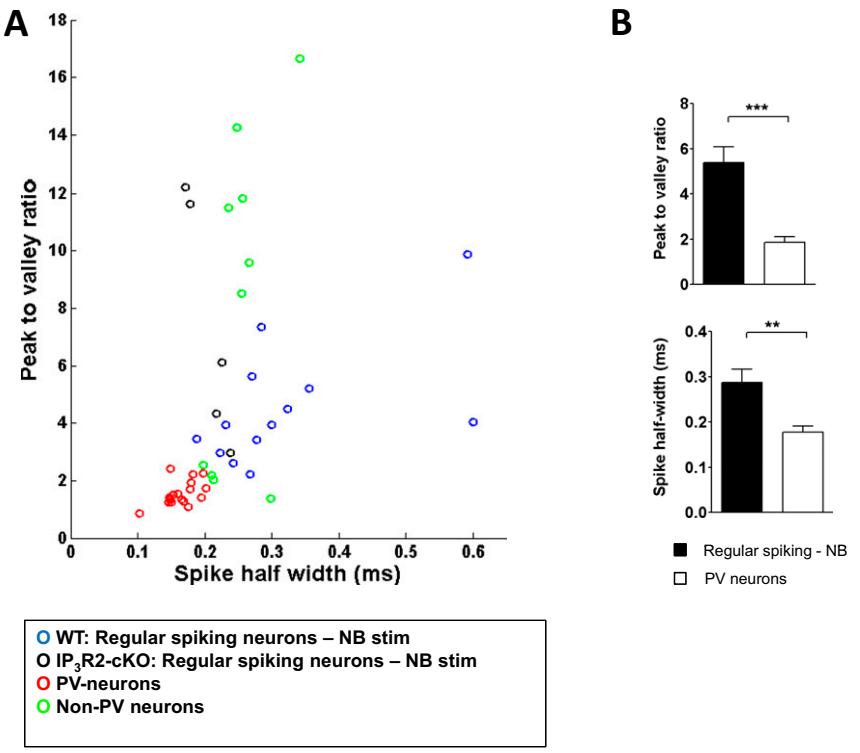

Fig. S1. Electrophysiological properties of neurons studied with cell-attached recordings in vivo. (*A*) Scatterplot of the mean peak-to-valley ratio of spikes and mean spike half-width recorded in individual regular spiking neurons and comparison with parvalbumin (PV)-expressing and non–PV-expressing neurons studied similarly in PV-Cre mice, where the PV-expressing neurons were labeled with RFP (3). (*B*) Population average of the mean peak-to-valley ratio and mean spike half-width in the regular spiking neurons and PV neurons. $^{**}P < 0.001$; $^{***}P < 0.0001$ by *t* test. Error bars indicate SEM.

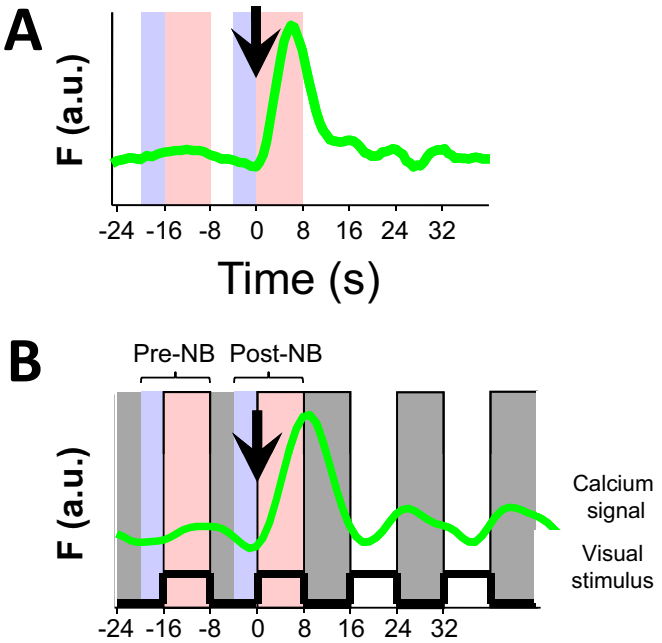

Fig. S2. Schematic shows calculation of post-NB and pre-NB responses, based on time course of responses in in vivo calcium imaging experiments without (*A*) and with (*B*) presentation of a visual stimulus. The black line indicates periods when visual stimulation was turned on and off. Pre-NB and post-NB responses were calculated in the time windows as indicated, using peak fluorescence value in the red time window (*A*) and mean fluorescence values across time points within the blue time window (*B*), such that Response = (A − B)/B·100. The arrow indicates the time point of NB stimulation. a.u., arbitrary unit.

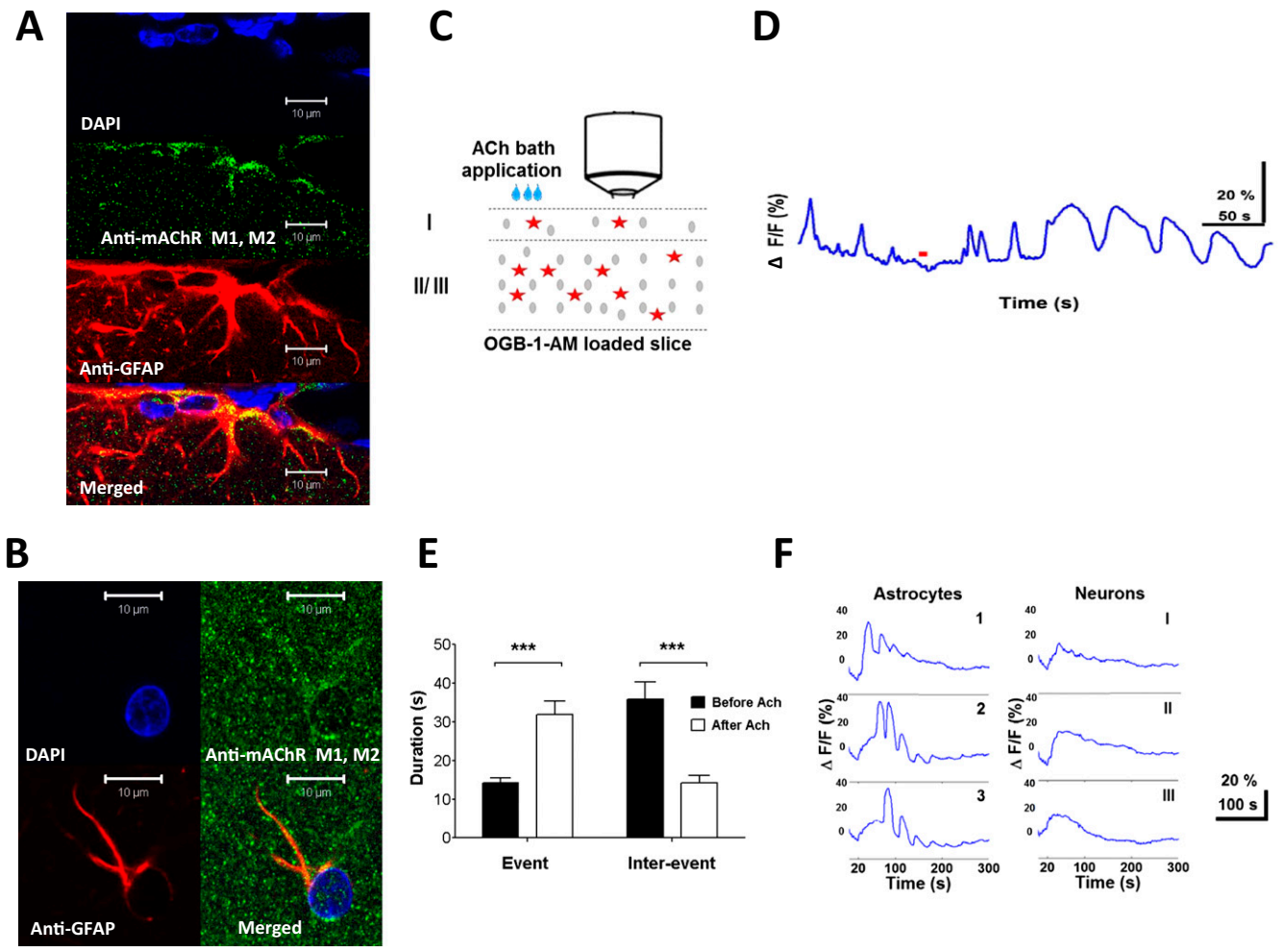

Fig. S3. Triple immunohistochemistry staining of astrocytes with DAPI (nuclear stain), antimuscarinic AChR (mAChR) M1/M2, and anti-GFAP shows colocalization of muscarinic receptors on astrocytes in layer 1 (*A*) and layer 2/3 (*B*). (*C*) Schematic shows simultaneous imaging of OGB1-AM–loaded astrocytes and neurons in layer 2/3 of V1 slices during bath application of ACh (10 mM). The ACh concentration remained constant throughout imaging. In spontaneously active astrocytes, bath application of ACh induced an increase in frequency (*D*) and duration (*E*) of spontaneous calcium transients (events), although decreasing the duration between them (interevents) (events: $n = 13$ astrocytes; $^{***}P < 0.001$, paired t test; interevents: $n = 12$ astrocytes; $^{***}P < 0.001$, paired t test). (*F*) ACh induces produces prolonged wave-like calcium increases in simultaneously imaged astrocytes. A prolonged, slow calcium elevation is evoked in neighboring neurons simultaneously with the initiation of calcium responses in astrocytes. Time of ACh bath application = 0; responses in this group of cells are initiated about 20 s later. The prolonged calcium elevation in neurons resembles the slow depolarization recorded in excitatory neurons by patch-clamp.

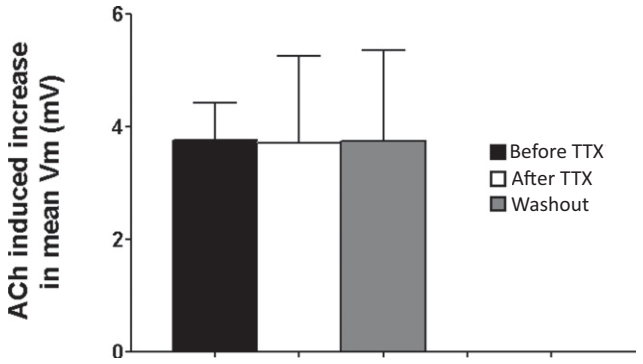

Fig. S4. Population average of ACh-induced increase in mean basal membrane potential (V_m) of neurons before/after bath application and washout of TTX (Before TTX/After TTX: $n = 10$ neurons; $P = 0.976$, paired t test; After TTX/Washout: $n = 10$ and $n = 4$ of 10 with washout attempted in 4 animals; $P = 0.991$, t test).

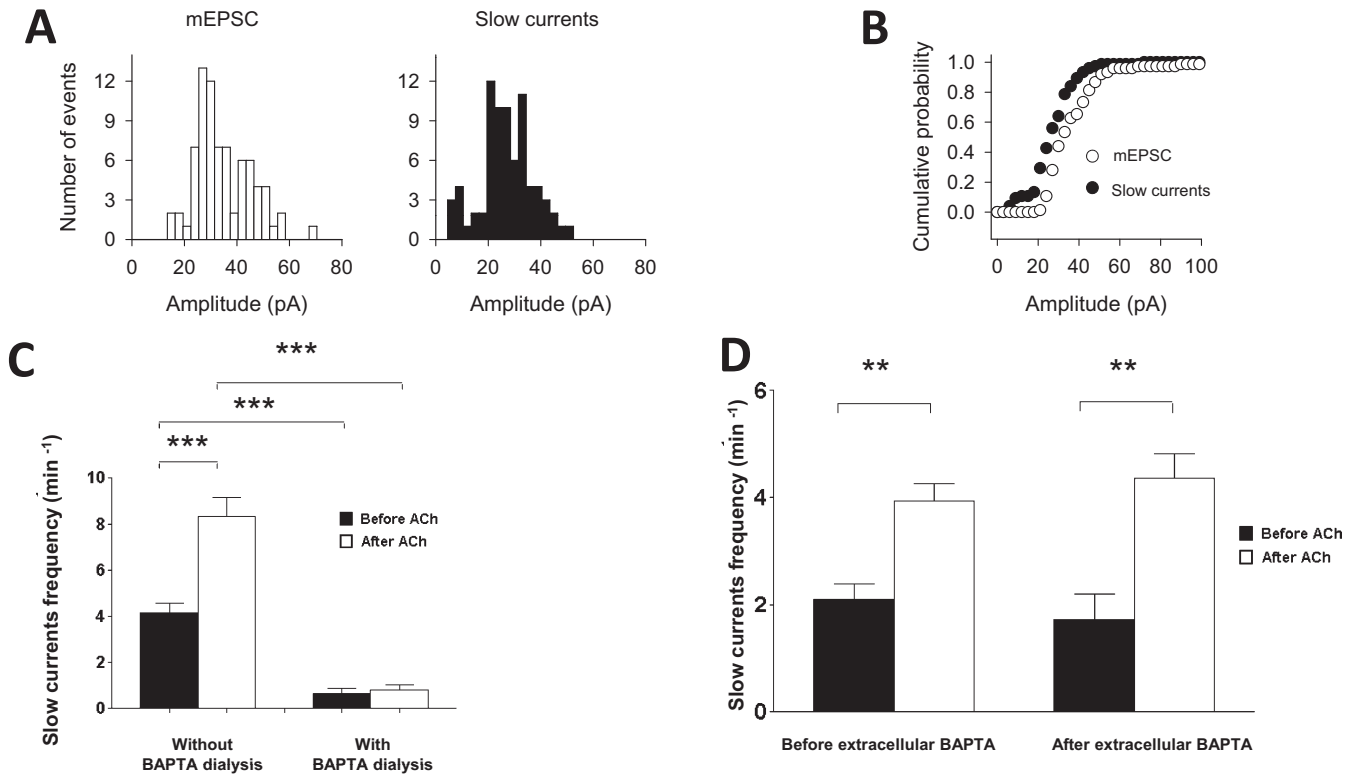

Fig. S5. (*A*) Histograms show the distributions of miniature excitatory postsynaptic current (mEPSC) and slow current amplitudes (bin width = 3 pA). (*B*) Cumulative probability plot of mEPSC and slow current amplitudes from *A*. (*C*) Population average of frequency of TTX-insensitive slow currents before and after ACh application in the presence and absence of BAPTA and A594 dialysis of the astrocyte syncytium. In the presence of BAPTA dialysis, the neuronal patch is obtained before and maintained throughout and after BAPTA dialysis (Fig. 4 *D* and *G*) or immediately after BAPTA dialysis (Without BAPTA, Before/After ACh: $n = 18$ in 9 animals; $P = 2.43E\text{-}06$, paired t test; With BAPTA, Before/After ACh: $n = 11$ in 8 animals; $P = 0.143$, paired t test; Before ACh, Without BAPTA/With BAPTA: $n = 18$ and $n = 11$; $P = 3.07E\text{-}06$, t test; After ACh, Without BAPTA/With BAPTA: $n = 18$ and $n = 11$; $P = 1.29E\text{-}7$, t test). $^{***}P < 0.001$; error bars indicate SEM. (*D*) Population average of frequency of TTX-insensitive slow currents evoked by ACh application, before and after extracellular BAPTA puff (Before extracellular BAPTA, Before/After ACh: $n = 7$; $P = 0.0022$, paired t test; After extracellular BAPTA, Before/After ACh: $n = 7$ and $n = 6$; $P = 0.0026$, t test; Before ACh, Before/After extracellular BAPTA: $n = 7$, $P = 0.229$, paired t test; After ACh, Before/After extracellular BAPTA: $n = 7$ and $n = 6$; $P = 0.446$, t test, 3 animals). $^{**}P < 0.01$.

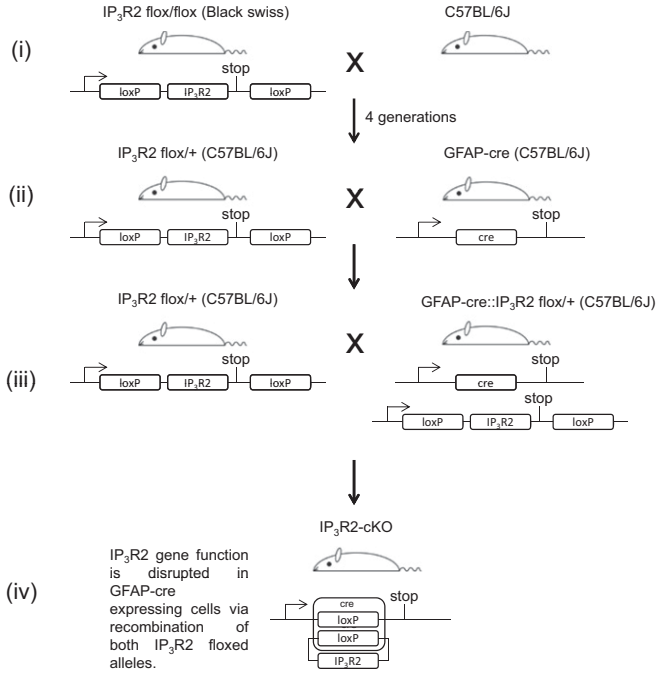

Fig. S6. Schematic diagram describes the generation of the IP_3R2-cKO mice. Further details are provided in *SI Materials and Methods, Mice*.

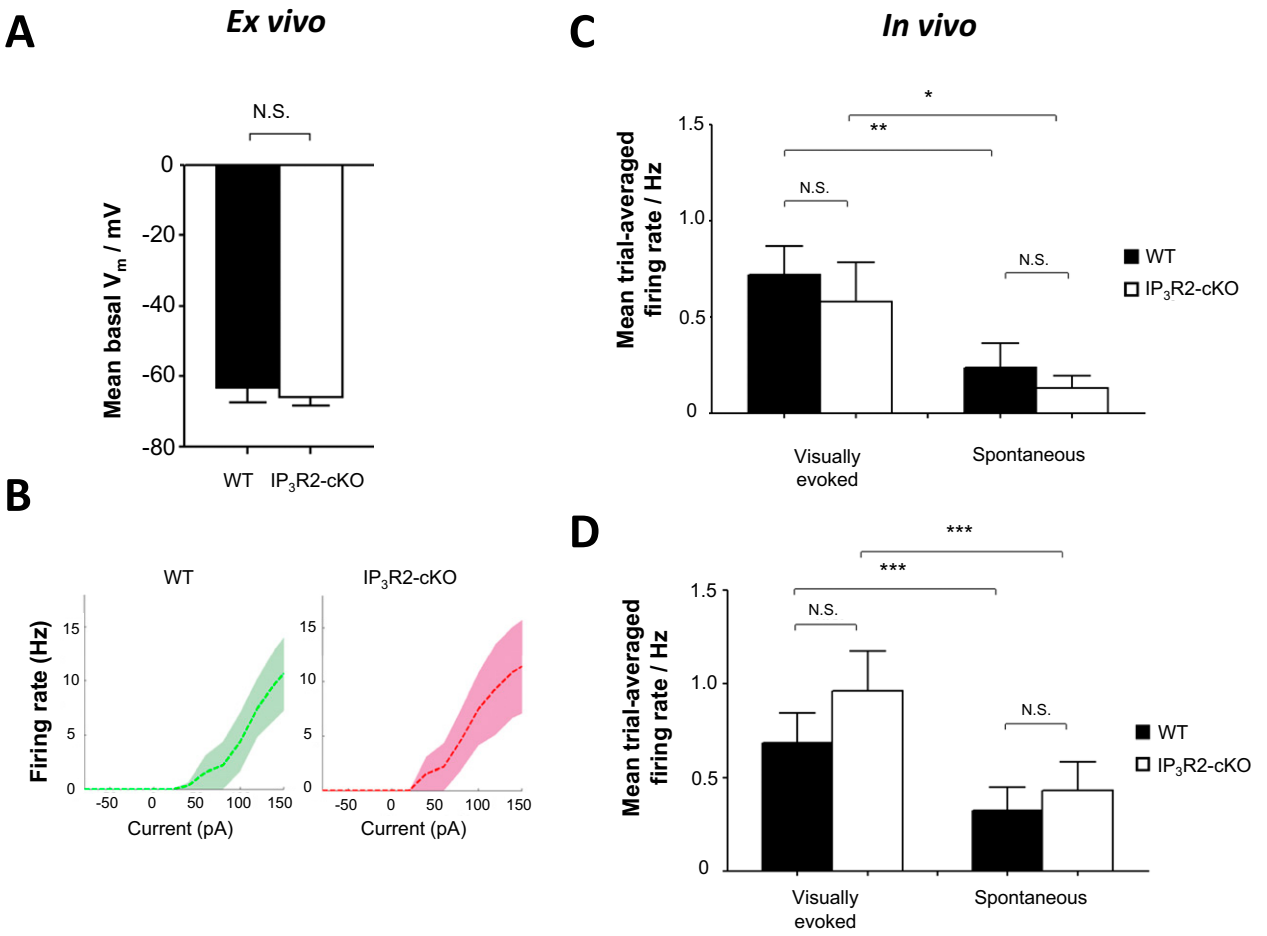

Fig. S7. (*A*) Mean basal membrane potential (V_m) of neurons recorded in Fig. 5*C* [$P = 0.615$, *t* test, comparing V_m of WT and IP_3R2-cKO neurons ($n = 5$ neurons each)]. (*B*) Mean firing rate-current curve of WT and IP_3R2-cKO neurons recorded in Fig. 5*C*. (*C*) Mean trial-averaged visually evoked and spontaneous responses of WT ($n = 6$ neurons) and IP_3R2-cKO ($n = 5$ neurons) regular spiking neurons recorded in Figs. 1 *E* and *F* and 5*D* [$P = 0.597$, *t* test comparing the visually evoked (ON responses) between WT and IP_3R2-cKO; $P = 0.476$, *t* test comparing the spontaneous (OFF responses) between WT and IP_3R2-cKO; $P = 0.0028$ and $P = 0.0460$, paired *t* test comparing the visually evoked (ON responses) and spontaneous (OFF responses) in WT and IP_3R2-cKO, respectively]. (*D*) Mean trial-averaged visually evoked and spontaneous responses of WT ($n = 41$ neurons) and IP_3R2-cKO ($n = 45$ neurons) regular spiking neurons recorded in Fig. 6 [$P = 0.305$, *t* test comparing the visually evoked (ON responses) between WT and IP_3R2-cKO; $P = 0.593$, *t* test comparing the spontaneous (OFF responses) between WT and IP_3R2-cKO; $P = 0.0002$ and $P < 0.0001$, paired *t* test comparing the visually evoked (ON responses) and spontaneous (OFF responses) in WT and IP_3R2-cKO, respectively]. N.S., nonsignificant. $*P < 0.05$; $**P < 0.01$; $***P < 0.001$.

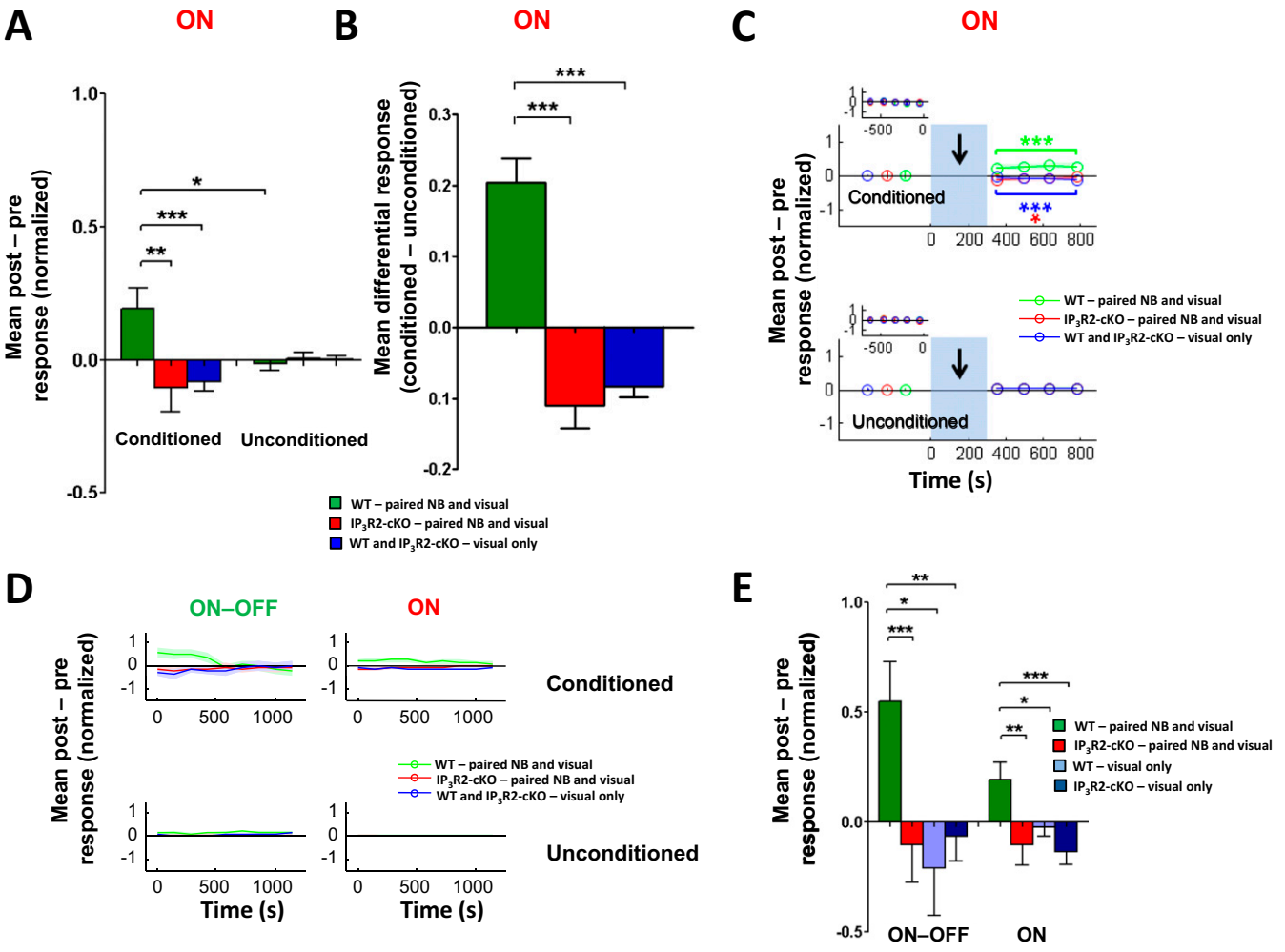

Fig. S8. (*A*) Population mean of normalized post-NB minus pre-NB responses (ON) at conditioned and unconditioned orientations in WT and IP_3R2-cKO in paired as well as visual-only control experiments. (*B*) Mean differential responses (conditioned − unconditioned orientations). ***$P < 0.001$ by the Wilcoxon rank-sum test. Error bars indicate SEM. (*C*) Time course of mean normalized post-NB minus pre-NB responses (ON) at conditioned (*Upper*) and unconditioned (*Lower*) orientations. Blue-shaded bars with an arrow indicate NB stimulation period. (*Insets*) Pre-NB baseline responses were averaged over four trials and are shown. Postpairing responses at the conditioned orientation were significantly enhanced in WT animals (green). Responses were suppressed in the visual-only condition (blue, $P < 0.001$) and in IP_3R2-cKO animals after pairing (red, $P < 0.05$). *$P < 0.05$; ***$P < 0.001$ by the Wilcoxon rank-sum test comparing responses before and after NB pairing. (*D*) Graphs similar to Fig. 6*D* and Fig. S8*C* plotted at a longer time scale to show the time course of recovery of ON and ON–OFF responses. The end of the NB stimulation period is indicated by 0 s. (*E*) Population mean of normalized post-NB minus pre-NB responses (ON–OFF and ON) at conditioned orientations in WT and IP_3R2-cKO animals, under different protocols (Fig. 6*C*, *Left* and *SI Materials and Methods*, *Single-Unit Recording*). *$P < 0.05$; **$P < 0.01$; ***$P < 0.001$ by the Wilcoxon rank-sum test.

Table S1. *P* values related to Fig. 4*G*

BAPTA (n = 5, paired t test, 4 animals)	Before BAPTA	Before/After ACh	$P = 0.0101$
	After BAPTA	Before/After ACh	$P = 0.410$
	Before ACh	Before/After BAPTA	$P = 0.0040$
	After ACh	Before/After BAPTA	$P = 0.0059$
Atropine (n = 10, paired t test, 5 animals)	Before Atropine	Before/After ACh	$P = 0.0035$
	After Atropine	Before/After ACh	$P = 0.753$
	Before ACh	Before/After Atropine	$P = 0.0797$
	After ACh	Before/After Atropine	$P = 0.0109$
D-APV (n = 10, paired t test, 7 animals)	Before D-APV	Before/After ACh	$P = 0.0008$
	After D-APV	Before/After ACh	$P = 0.543$
	Before ACh	Before/After D-APV	$P = 0.0004$
	After ACh	Before/After D-APV	$P = 0.0001$

D-APV, D-2-Amino-5-phosphonovaleric acid.

Table S2. *P* values related to Fig. 6*C*, *Left* and Fig. S8*A*

	ON	ON–OFF
A_trained/B_trained	0.00220	0.000500
A_trained/C_trained	0.000600	0.00120
A_trained/A_untrained	0.0166	0.00640
B_trained/C_trained	0.422	0.827
B_trained/B_untrained	0.230	0.0563
C_trained/C_untrained	0.0311	0.169
A _untrained/B_untrained	0.813	0.385
A_untrained/C_untrained	0.477	0.248
B_untrained/C_untrained	0.634	0.674

The Wilcoxon rank-sum test was used. A indicates WT, NB and visual; B indicates IP_3R2-cKO, NB and visual; and C indicates WT and IP_3R2-cKO, visual-only.